CONTRIBUTION OF KNET AND KIK-NET DATA TO THE MONITORING OF NONLINEAR PROPERTIES OF THE SHALLOW CRUST

Luis Fabian Bonilla[1], Philippe Guéguen[2], Céline Gélis[3]
1 Senior researcher, GERS-SRO, Univ. Gustave Eiffel, Marne-la-Vallée, France
(luis-fabian.bonilla-hidalgo@univ-eiffel.fr)
2 Senior researcher, ISTerre, Univ. Gustave Eiffel, IRD, CNRS, Univ. Savoie Mont Blanc, Univ. Grenoble Alpes, Grenoble, France (philippe.gueguen@univ-grenoble-alps.fr)
3 Senior researcher, IRSN, Fontenay-aux-Roses, France (celine.gelis@irsn.fr)

ABSTRACT

KNET and KiK-net stations, installed since the middle of the 90's and the beginning of 2000, respectively, embrace a large database of earthquakes produced by different types of tectonic regimes and recorded on various soil conditions all over Japan. Around 1000 KNET stations are deployed at the ground level; whereas, near the 700 deployed KiK-net stations comprise both surface and borehole instruments located mostly between 100 and 200 m depth. Furthermore, all sites have the P and S wave velocities in the first 20 m for KNET and up to the borehole depth for KiK-net, respectively. NIED, the local agency operator in Japan, has made all these data freely available with a common format for all records. All these features make that these data are of great importance when studying site effects under different site conditions and ground motion levels. One of the key features in earthquake engineering is the evaluation of nonlinear site response, which happens when the strength of the soil is relatively low with respect to the amplitude of the incoming wavefield. Nonlinear soil behavior is commonly studied using laboratory data where the evolution of shear modulus and damping ratio as a function of shear strain are measured. The recent developments in Seismology in robust signal processing tools to study Earth's noise wavefield and the related velocity changes due to perturbations of the dynamic stress field can also be used on earthquake data. Indeed, velocity changes can directly be transformed into shear modulus changes. More importantly, these measurements are made in situ, thus averaging the local behavior over a soil volume. In this article, we present results using cross and auto-correlation methods to extract velocity and frequency changes exploiting 17 years of earthquake data recorded at station IBRH16 (KiK-net). We show the healing after the Tohoku sequence in 2011. Moreover, the observed fluctuation of velocity and frequency changes in the background seismicity suggests that the site response variability may be strong and very sensitive at the predominant frequency of the site. This can be of great importance when using single-station sigma on empirical ground motion models in site-specific seismic hazard studies. Finally, we present the spatial distribution of nonlinear site response from the M7.1 Honshu earthquake in February 13, 202.

Keywords: seismic site effects, velocity changes, nonlinear site response, Tohoku

INTRODUCTION

The top few hundred meters of the crust is a very complex environment, involving different type of materials having various degrees of cracking, damage and subjected to ongoing weathering processes and fluid migration. The prevalent pre-existing damage, low seismic velocities that amplify ground motion, and low confining stress make the material in the top crust highly susceptible to additional failures, especially during strong earthquake ground motion. Furthermore, damaged rocks with cracks and other defects are known to exhibit nonlinear elasticity manifested by shifts of the resonance frequency with increasing loading amplitude and related phenomena. Indeed, nonlinear response to loadings and failure processes have been reported in various laboratory experiments (i.e. Johnson and Jia 2005; Pasqualini et al., 2007; TenCate, 2011; Lieou et al., 2017). Therefore, *in-situ* analyses of nonlinear material behavior and temporal changes of seismic properties are essential to better understand wave propagation in the top crust, and correctly estimate the related seismic hazard.

The deployment of dense arrays worldwide and the development of robust signal processing methods allow measuring small velocity variations due to dynamic perturbations at the crustal scale (i.e. Brenguier et al., 2008; Wang et al., 2019). The analyses generally use ambient seismic noise, which is wide spread and is available in essentially all regions and time intervals (i.e. Sens-Schönfelder and Wegler 2006; Brenguier et al., 2008, 2014). However, noise sources are relatively weak, so noise-based analysis requires stacking of relatively quiet periods, leading to analysis time steps of days or more. Seismic signals generated by repeating earthquakes have also been used to derive temporal changes of seismic velocities (i.e., Poupinet et al. 1984), and also involve time steps of days. The use of spectral ratios of seismograms recorded by different stations (i.e. Wu and Peng, 2012; Nakata and Snieder, 2012), cross-correlations of earthquake waveforms (Roux and Ben- Zion, 2014), and auto-correlation in moving time windows of seismograms (Bonilla et al. 2019; Qin et al. 2020; Bonilla et al., 2020) can achieve time resolution of minutes to seconds and resolve finer details of temporal changes.
In this study we use seismic interferometry and auto-correlation functions to compute co-seismic velocity and frequency changes for data recorded at station KiK-net IBRH16 since the beginning of its operation in 2003 until the end of 2020. We compute velocity changes as a function of frequency, and we find that the shallow crust has a resonance frequency, which is particularly sensitive to the intensity of the ground shaking in a similar way to what is shown by laboratory experiments (i.e. Pasqualini, 2007). We use this property to monitor the spatial distribution of nonlinear material response during the M7.1 Honshu earthquake of February 13, 2021.

DATA AND METHODS

In the following, we analyze data recorded at the KiK-net station IBRH16. This station has one sensor at GL-0m and another at GL-300m, and it was studied in Bonilla et al. (2019) to obtain the co-seismic velocity and frequency changes during the Tohoku-Oki M9.0 earthquake in March 2011. We collected data recorded at this station since the beginning of its operation in 2003 until the end of 2020. The data include events with a magnitude range from 3 to 9, having a peak ground acceleration (PGA) greater than 1 cm/s^2 recorded at the surface instrument. Figure 1 shows the map of all events used in this study. There is a good azimuthal coverage, and no distinction of crustal or subduction events has been made.

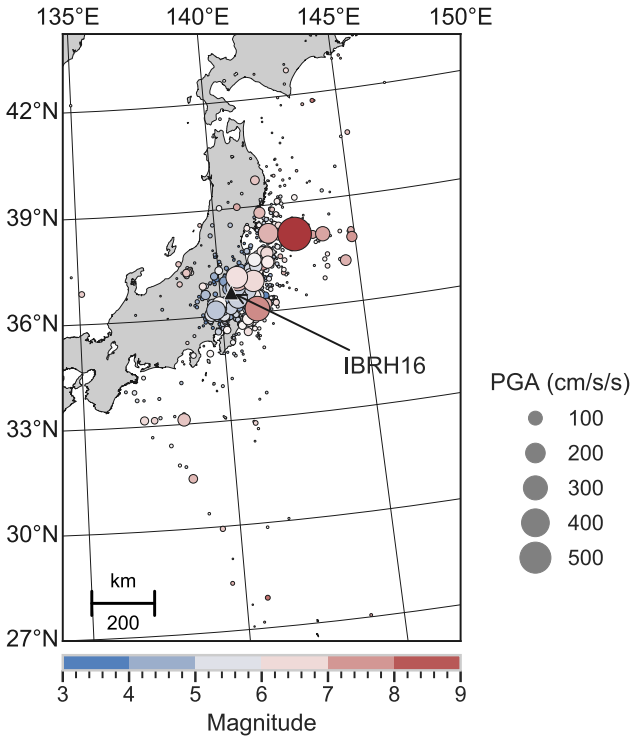

Figure 1. Map showing the location of KiK-net station IBRH16 and the epicenters of earthquakes between 2003 and 2020 recorded at this site. The symbol size represents the PGA recorded at station IBRH16.

Figure 2 (left) displays the magnitude-distance-PGA distribution of the data, where the maximum PGA is about 600 cm/s^2 produced by the Tohoku-Oki M9 event. The data span mostly between 10 and 1000 km from the station. Figure 2 (center) shows the P and S-wave velocity profile (Okada et al., 2004). The associated Vs30 (i.e., harmonic average shear-wave velocity in the first 30 m) is 626 m/s, which can be considered as stiff soil. However, the top 12 m has a harmonic average shear-wave velocity of 342 m/s overlaying stiff material (Vs > 1400 m/s). The combination of layers having a low-velocity close to the surface and a relatively strong impedance contrast may favor nonlinear soil behavior in case of strong ground shaking caused by the combined effect of low soil strength and wave amplification, respectively (Bonilla et al., 2011; Régnier et al., 2013). Figure 2 (right) illustrates the spectral ratio between these two sensors using data recorded between 1998 and 2009 having PGA values less than 10 cm/s^2 at the surface (Bonilla et al., 2011). They assume that such weak ground motion may not induce nonlinearity and the response shows that the fundamental and predominant frequencies are 1.8 and 7 Hz, respectively. Taking a homogeneous layer of 12 m thickness and a Vs of 342 m/s, the resonance frequency is 7.1 Hz. This suggests that the first 12 m are responsible for the predominant frequency observed in Figure 2 (right).

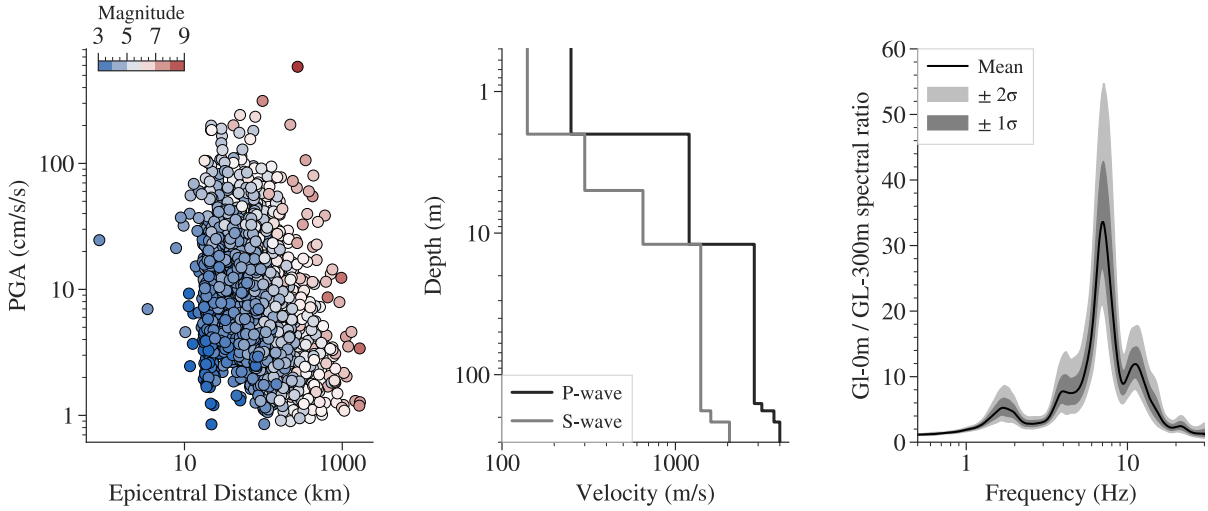

Figure 2. (left) Magnitude-distance-PGA distribution. (center) P and S velocity profiles at IBRH16. (right) Spectral ratio using data having a PGA < 10 cm/s^2.

Seismic interferometry

The impulse response function (IRF) computed by deconvolution, using data recorded simultaneously at two sensors, is the so-called seismic interferometry (Wapenaar et al., 2010; Nakata and Snieder, 2012). This operation permits to obtain the travel time of waves between the stations. Bonilla et al. (2019) used overlapping time windows to compute the travel time between the surface and borehole records at station IBRH16. They observed longer travel times and lower predominant frequency values as the intensity of the ground motion increases. Such variation of travel times is due to changes of the velocity media between the two sensors that reflect nonlinear material behavior.

In this study, we compute the impulse response of each recorded event between the pair of stations using a 5 s time window centered at the PGA of the surface record. In order to increase the signal-to-noise ratio we stack the IRF's as a function of the PGA of the event in bins of [<10], [10-25], [25-50], [50-100], [100-200], [200-300], [300-400], and [>400] cm/s^2, respectively. Figure 3 (top) shows the stacked interferograms at different PGA bins. The reference is the surface station so that they show the incident and reflected wavefield, acausal and causal part, respectively. One clearly sees the increase of the travel times as the PGA increases passing from around 0.2 s at PGA < 10 cm/s^2 to 0.3 s at PGA > 400 cm/s^2 in the acausal time series. For clarity, the IRF's are filtered between 1 and 10 Hz. In order to retrieve the resonance frequencies, we need to compute the inverse of the FFT amplitude of the acausal IRF's. This is equivalent of having the borehole station as reference. Figure 3 (bottom) shows the variation of the resonance frequencies as the intensity of the ground motion increases. We observe a reduction from 17 Hz to 12.5 Hz, and from 7.5 Hz to 3 Hz. Notice how the higher frequencies are completely wiped out

for the PGA > 400 cm/s^2 (Tohoku record). We see that the 7 Hz predominant frequency from Figure 2 is the one sensitive to these changes. This suggests that the first 12 m of soil at station IBRH16 are prone to nonlinear material behavior.

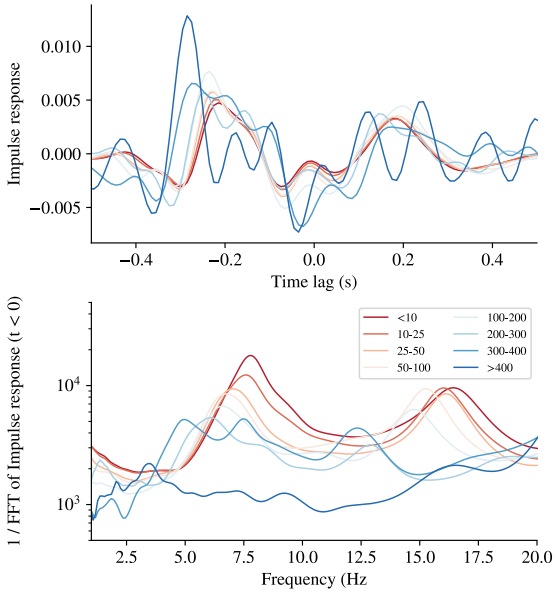

Figure 3. (top) Stacked interferograms at different PGA bins and filtered between 1 and 10 Hz. Notice the increasing travel times in the acausal part from 0.2 to 0.3 s approximately. (bottom) Inverse of the FFT amplitude of the acausal interferogram. Notice the decrease of the resonant frequency from 7.5 Hz (PGA < 10 cm/s^2) to around 3 Hz (PGA > 400 cm/s^2).

Autocorrelation functions

Following Claerbout (1968), a reflection seismogram at a site can be obtained from the autocorrelation of the recorded earthquake waveforms, and Wapenaar (2003) generalized this conjecture to three dimensions. Bonilla et al. (2019) and Bonilla and Ben-Zion (2020) computed autocorrelation functions (ACF) on earthquake data to assess velocity and frequency changes in the shallow crust since it is more common to have surface stations than vertical arrays.

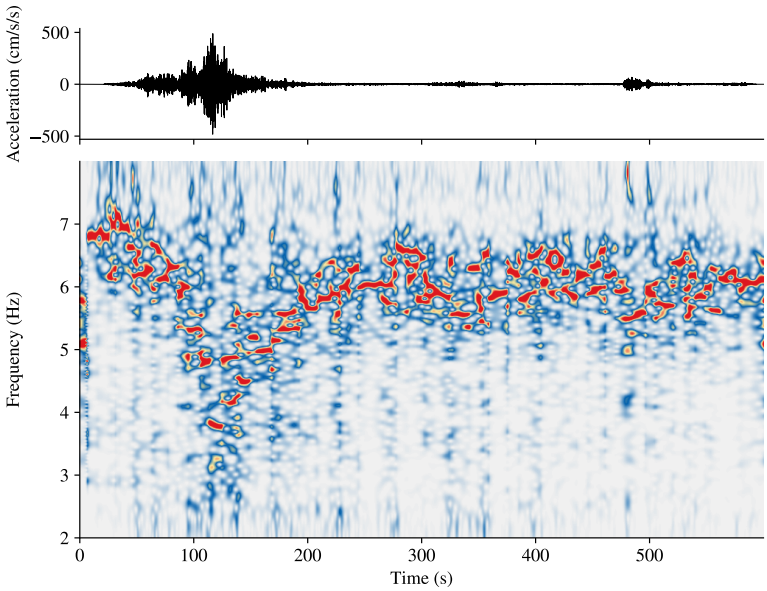

Figure 4. (top) Composed accelerogram from Tohoku-Oki M9 event recorded at IBRH16 GL-0m, EW component. (bottom) Spectrogram computed with the generalized Stockwell transform between 2 and 8 Hz. Notice the strong frequency shift around 100 s and the recovery that takes place after the strong motion ceases. The material is not completely healed after 10 min of shaking as we still see a lower resonance frequency compared to the beginning.

Figure 4 (top) shows the EW surface record of the Tohoku-Oki M9 event that was recomposed from two consecutive files. We can see the mainshock and two aftershocks around 300 s and 500 s, respectively. The figure below displays the spectrogram computed using the generalized Stockwell transform (Sattari, 2017). This technique allows to extract, with high resolution, the time evolution of the predominant frequency. It begins around 7 Hz at low amplitude PGA values and coincides with the result from the spectral ratio in Figure 2. Then, there is a drop of this frequency to nearly 3 Hz, and it recovers, up to around 6 Hz, after 100 s approximately. There is no full recovery after 10 min of data. Bonilla et al. (2019) studied this record and obtained up to 60% velocity changes during the strongest ground motion between 1 and 12 Hz.

In order to better see what frequencies are involved in this process we need to perform a time-frequency analysis. Bonilla and Ben-Zion (2020) studied a dense array in one branch of the San Jacinto fault, and found that the velocity and frequency changes depend on the frequency band analyzed. They used four frequency bands where the lower and upper frequencies were one octave one from each other (i.e. a factor of two between frequencies). We compute the ACF for 5 s time windows centered around the PGA and stack them following the same PGA bins proposed for the IRF's. The ACF's are obtained using the phase correlation method developed by Schimmel (1999). This technique has the advantage of using only the phase information of the analytical signal, so it is not necessary to perform any bit normalization nor pre-whitening the data. Ventosa et al. (2019) showed that the method of Schimmel (1999) can be computed in the frequency domain, making its calculation very fast and inexpensive. However, this time we evaluate the velocity and frequency changes for 100 frequencies, each being the center of one octave. The frequency range is 1.0 to 25 Hz and equally spaced in a logarithmic scale. We use the generalized Stockwell transform to extract filtered ACF's at each center frequency and then compute the velocity change using the stretching technique (i.e. Sens-Schönfelder and Wegler, 2006). Concomitantly, we compute the predominant frequency of the filtered ACF's.

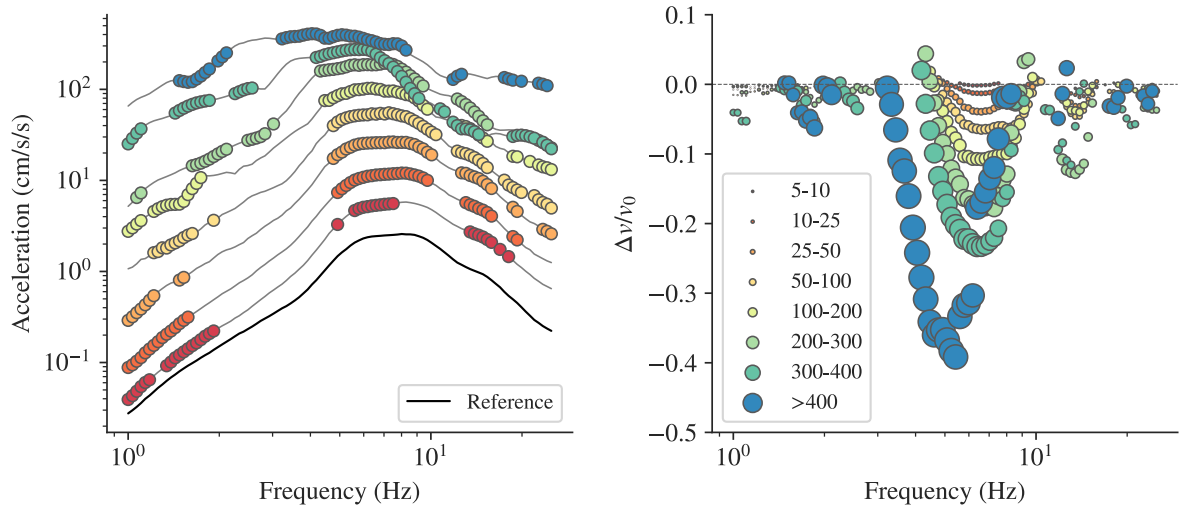

Figure 5. (left) Average acceleration values from filtered records and grouped in PGA bins per frequency. The solid black line represents the reference, i.e. PGA values less than 5 cm/s^2. (right) Velocity changes as a function of frequency computed between the stacked ACF's per PGA bin and the reference ACF. The PGA bins are shown in the legend in cm/s^2, and the symbol size is proportional to the PGA in the bin.

Figure 5 show these results. On the left, there is the evolution of the resonance frequency as a function of the PGA bin. Lower acceleration values show higher resonance frequencies. We clearly see that these curves show a similar behavior as the results obtained from resonant column experiments in soils (Ishihara, 1996), and in rock samples to study their nonlinear elastic properties (i.e. Pasqualini et al, 2007; TenCate, 2011). This result suggests that the soil is sensitive at a particular resonance frequency, which happens to be the predominant frequency observed in Figure 2. In other words, we can imagine a soil column being resonated during an earthquake as a soil sample in the resonant column in the

laboratory. If the resonance frequency changes as a function of the intensity of the ground motion, there is nonlinear material behavior.
If we compute the velocity changes per center frequency between each stacked ACF and the reference we obtain Figure 5 (right). This figure clearly illustrates the increase of velocity changes around the predominant frequency of 7 Hz. The larger the intensity of the ground motion, the larger the velocity change, and the lower the resonance frequency becomes. If we add the information of which frequencies are reduced during material nonlinearity (color circles in Figure 5 left); they all coincide at the peak of the ground motion acceleration. Therefore, this method allows to localize the resonance frequency sensitive to nonlinear behavior.

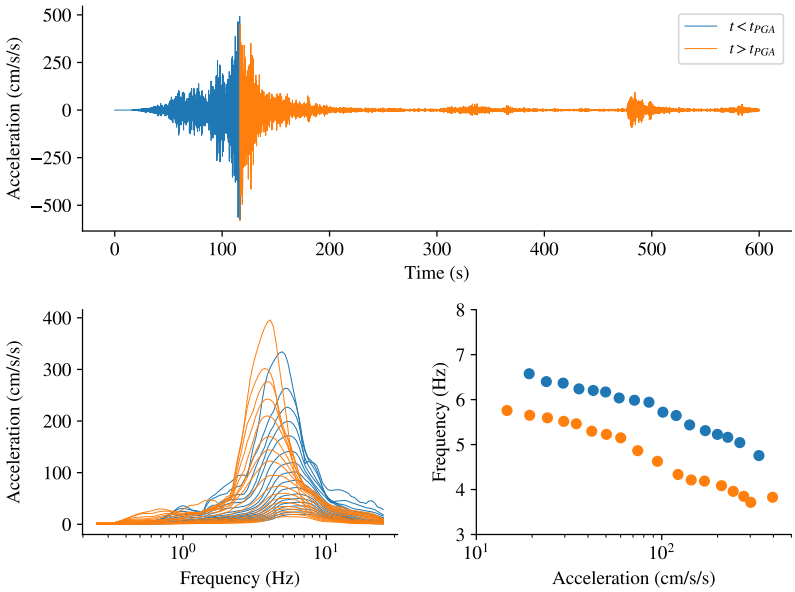

Figure 6. (top) Tohoku-Oki and aftershocks recorded at the EW surface instrument. The colors separate data before and after the PGA, respectively. (bottom left) Resonance curves as a function of acceleration. (bottom right) Peak resonance frequencies as a function of acceleration. Notice the difference of about 1 Hz between the beginning and the end of the ground shaking.

As an example of this method, we compute the resonance curves on the Tohoku-Oki and aftershock records (Figure 6) for 100 frequencies between 0.25 and 25 Hz. We separate the loading/unloading cycles before and after the PGA. We see that the former has higher peak resonance frequencies than the latter. This was also found by Bonilla et al. (2019) using ACF's on moving time windows. This result shows that there is degradation during the strong motion, which might be caused by damage or pore pressure effects, or both. This is still a research subject to develop.

RESULTS AND DISCUSSION

Monitoring frequency changes at permanent seismic stations

Seeing the effect of earthquake ground shaking as a resonance effect on soils allows to exploit the recorded data at any given station. This is done with all available records between 2003 and 2020 at station IBRH16. We compute the resonance peak frequencies for a time window of 5 s centered around the PGA and we plot them as a function of time, event magnitude, and PGA (Figure 7).

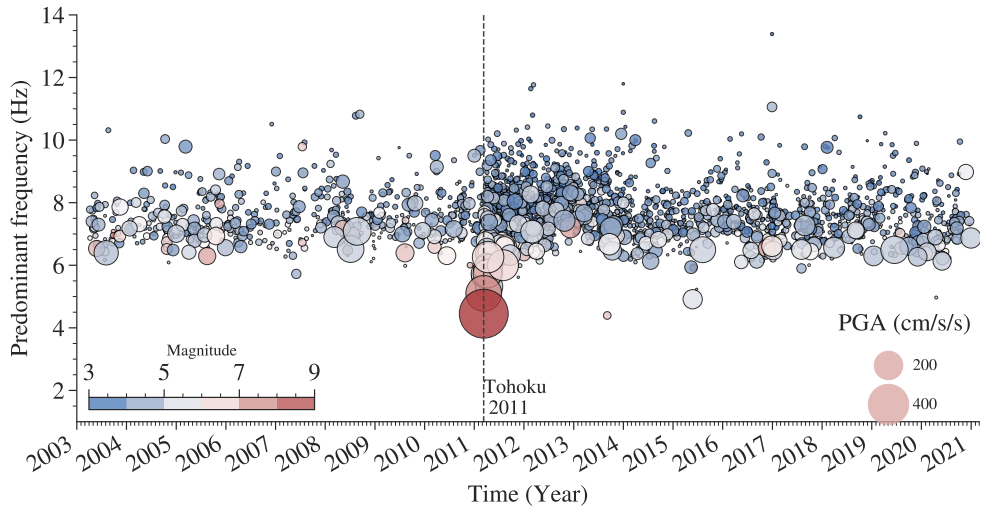

Figure 7. Evolution of the predominant frequency for earthquakes recorded at the EW surface component of station IBRH16. Data span since the beginning of the station operation until the end of 2020. Notice the cluster activity after the Tohoku-Oki M9 earthquake.

Results shown in Figure 7 do not need any reference as it is the case when computing velocity changes. There is a clear frequency shift produced during the Tohoku-Oki M9 event and the subsequent aftershock activity. These frequency changes are co-seismic for all earthquake data. There is a large variability of the site response around the predominant frequency, which is related to the first 12 m depth of soil. This result indicates that even if Vs30 is known, there is a variability of the velocity within the soil column that is not negligeable (coefficient of variation of 11%), which is usually unknown and not taken into account in site-specific seismic hazard analyses. The use of single-station sigma may also be compromised. Yet, this is mainly observed at one frequency. Thus, more studies need to be conducted to understand the physics behind such frequency changes and their effect in site response assessment.

Shallow crust healing at IBRH16 site after the Tohoku-Oki M9 mega-earthquake

Figure 7 shows a strong effect of the Tohoku-Oki M9 event activity on the frequency response of station IBRH16. To better assess the phenomenon of healing observed after dynamic transients, we evaluate the velocity changes as a function of frequency for all events. In this case, the reference ACF is the stack of ACF's for earthquakes having a PGA < 5 cm/s^2. As before, we conduct this computation for a subset of the 100 center frequencies, namely between 3 and 10 Hz. This is to reduce computation time and also because previous results indicate that the velocity and frequency changes are concentrated around 7 Hz. Figure 8 shows the velocity changes for these center frequencies, and in order to better see the healing, the data are ordered in time with respect to the onset of the Tohoku-Oki M9 earthquake. Only data showing negative frequency shifts are shown here. This is the reason why we see negative velocity changes all the time. To ease the visualization of the time recovery, we compute the mean of the data (gray dots) for variable time windows and we plot the corresponding error estimates (red dots). First of all, the time recovery is seen in the frequency band between 6 and 8 Hz. Almost full recovery with respect to the background seismicity is nearly 90 days after the mainshock for the center frequencies of 6, 7, and 8 Hz. Higher frequencies recover faster, after 20 days approximately. This suggests that there is a depth dependency of the perturbation after a large event, and the shallower part recovers faster than the deeper part. This has also been seen in small amplitude events in California (Bonilla and Ben-Zion, 2020). Another interesting thing is that the velocity changes at these particular frequencies are at most 20%, much lower than the 60% found by Bonilla et al. (2019) who studied these effects for a broadband effect between 1 and 12 Hz. The use of a single frequency band mixes the effects produced at different wavelengths. This suggests that time-frequency analyses should be done to better identify the frequencies/wavelengths that are involved in such changes, and for a better assessment of the shear modulus reduction using this technique.

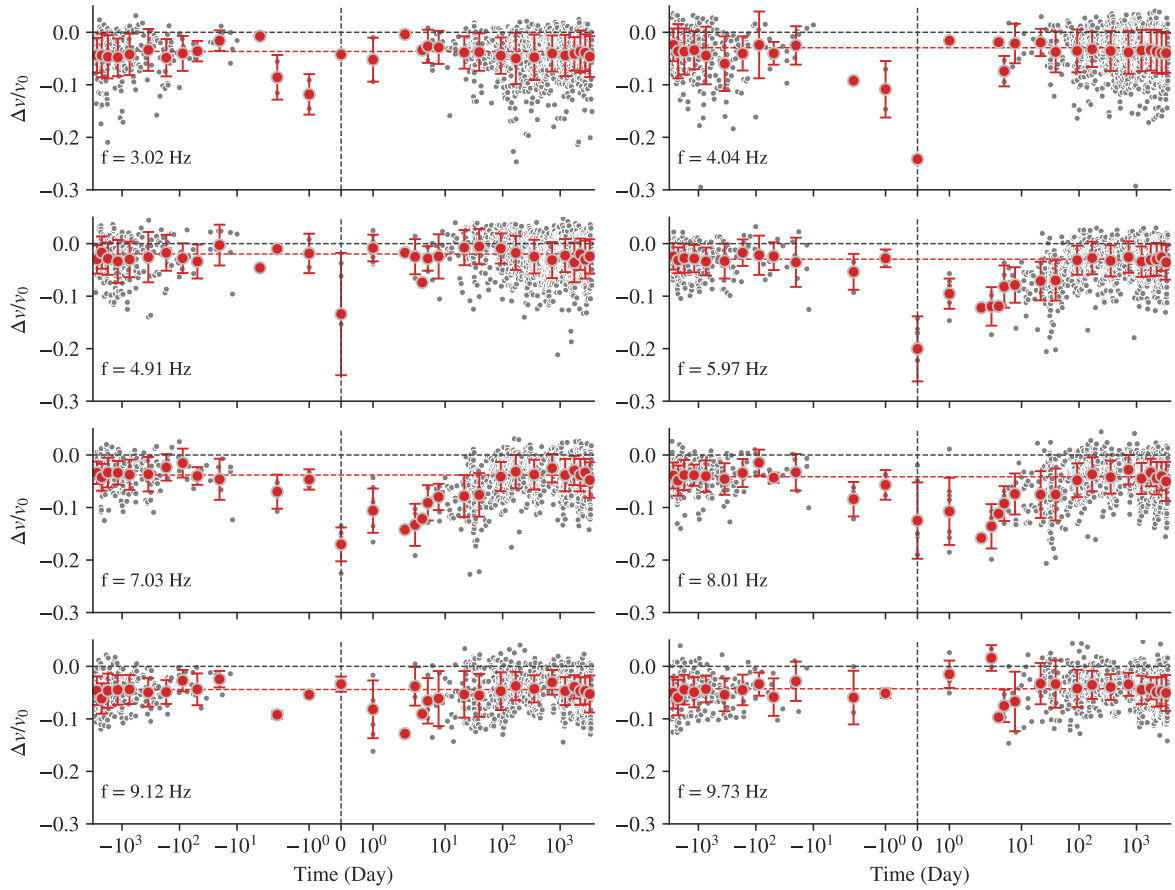

Figure 8. Velocity changes at selected frequencies between 2003 and 2020 at IBRH16. The origin of the time scale is centered at the time of the Tohoku-Oki M9 earthquake.

Spatial distribution of nonlinear effects: the M7.1 Honshu earthquake of February 13, 2021

We have seen that it is possible to obtain the time evolution of the resonance frequency for a single station. In what follows we use the same technique to study the spatial distribution of nonlinear site response by using the records of the M7.1 Honshu earthquake of February 13, 2021. To do that we need to estimate the reference value for each station to compute the related frequency change. This means, we compute a proxy of the nonlinear site response using the frequency shift instead of the velocity change. This is because it is much faster than computing velocity changes for a set of center frequencies as it was done in Figure 8. We therefore follow the procedure depicted in Figure 6, where we compute the resonant frequency peaks, but only between the beginning and 20% after the PGA. We are interested in the largest frequency change. However, we could also see the difference between the beginning and the end of the earthquake, meaning full recovery or not of the site after the end of shaking. We obtain the frequency corresponding to the largest PGA bin, which we call f_p, and the reference is computed as the weighted average of the resonance curves for PGA values less than 50 cm/s^2. This is called f_{p0}. Finally, we estimate the frequency changes as $\Delta f_p / f_{p0}$, and $\Delta f_p = f_p - f_{p0}$.
Figure 9 illustrates the frequency changes computed at KNET and KiK-net stations that recorded the NS components of the M7.1 Honshu event. We selected this component direction because it displays the largest acceleration at station MYGH10 (1425 cm/s^2). We plot only the stations that suffered negative frequency changes, which indicates nonlinear material behavior. As expected, the largest changes, more than 50%, are near the epicentral area. However, there is a non negligeable number of stations showing different degrees of nonlinear soil response up to 300 km epicentral distance, approximately.

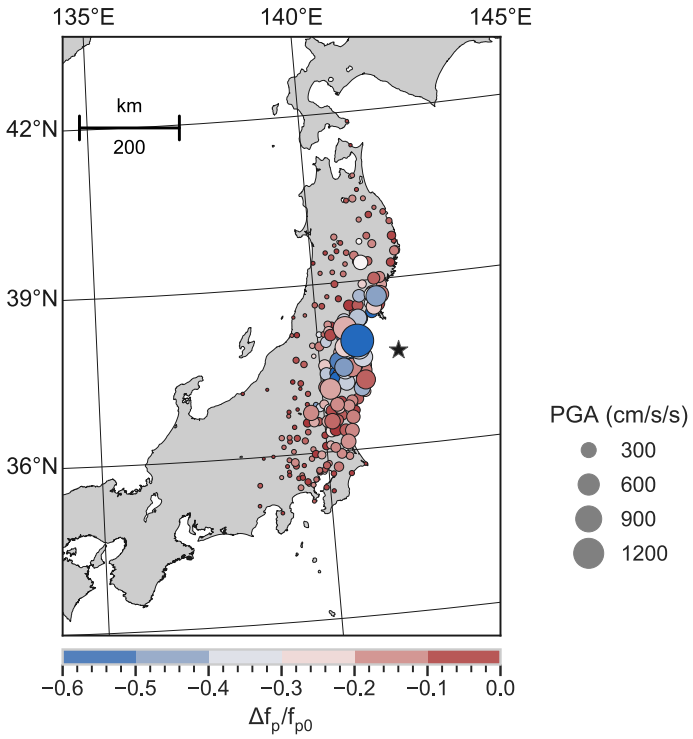

Figure 9. Frequency changes for the M7.1 Honshu earthquake of February 13, 2021.

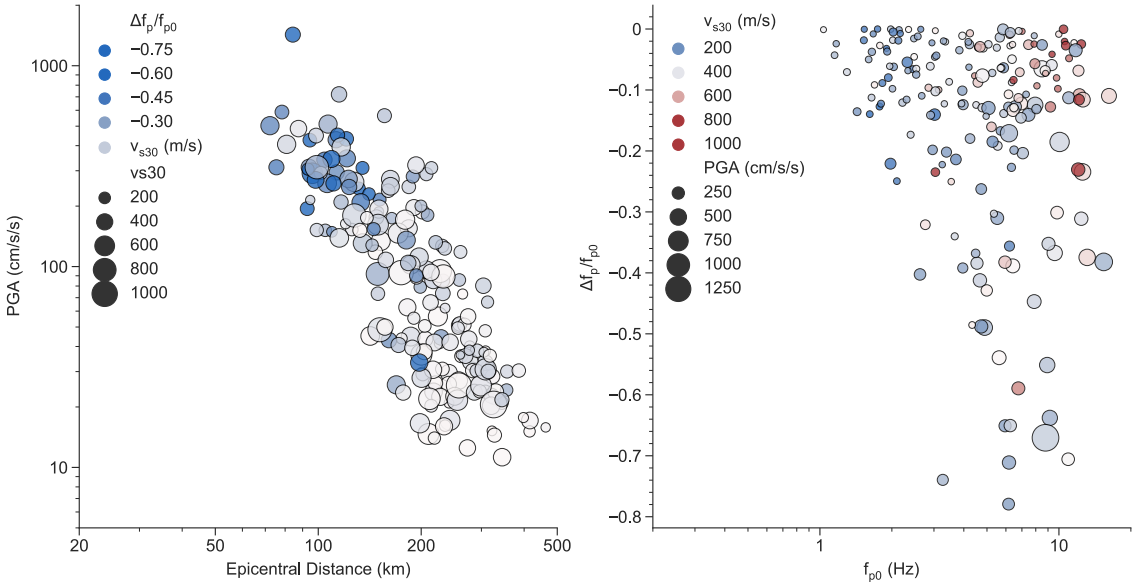

Figure 10. (left) Frequency shift as a function of PGA, distance and Vs30 conditions. (right) Frequency shift as a function of the reference resonance frequency, Vs30 and PGA. Both figures are for data from all KNET and KiK-net stations that recorded the M7.1 Honshu earthquake of February 13, 2021

Another representation of the results is shown in Figure 10 (left), which illustrates the frequency shift as a function of PGA, distance, and Vs30. It exhibits the spatial extension of nonlinear soil effects (frequency changes > 30%) up to 200 km. The Vs30 associated to these phenomena can go up to more than 600 m/s. Figure 10 (right) displays the frequency shift as a function of the reference resonance frequency, Vs30 and PGA. Sites having resonance frequencies larger than 5 Hz and Vs30 values close to 500 m/s have the largest frequency shift. On the contrary, sites with low resonance frequencies, less than 4-5 Hz, and even for low Vs30 values, show a smaller nonlinear effect (frequency changes < 10%). Yet, this need to be studied with more earthquakes to see whether this is an effect of sites being too far

from the epicentral area. However, sites having a high Vs30, larger than 600 m/s, and a resonance frequency around 10 Hz, also present frequency shifts around 10-20%. An analysis similar to station IBRH16 should be done at those sites to see whether shallow low velocity layers might be responsible for this behavior. These results explore if the reference resonance frequency is correlated to Vs30, and possibly to use it as a proxy for site characterization when computing ground motion models (i.e. Zhao et al., 2015; Di Alessandro et al., 2012).

CONCLUSIONS

In this study we use seismic interferometry and auto-correlation functions to compute frequency dependent velocity changes using earthquake data. We find that the site is sensitive to a particular resonance frequency, which is modifed during strong ground motion. Using this property we follow its time evolution as a proxy of nonlinear material behavior. An advantage is that no reference is needed to obtain the resonance frequency, and it permits monitoring a particular site for the changes affecting the associated wavelength. Nonetheless, calculating velocity changes as a function of frequency remains the most complete tool to investigate the shallow crust response. An important issue is the temporal changes of the crust response. The resonance frequency clearly identifies a long perturbation after the Tohoku-Oki M9 earthquake, which seems to last until the end of 2014. Conversely, velocity changes show a faster recovery, in the order of months around the same frequency value. These needs further research. We have shown results for one component only, usually the one that presented the largest recorded motion; however, it is possible to compute all three components giving an empirical framework of observed nonlinear behavior in 3D. The variability of the resonance frequency at IBRH16, coefficient of variation of 11%, and the fact that it is related to depths shallower than 30 m, illustrates the inadequacy of Vs30 to properly characterize a site. These observations also question the single-station sigma seismic hazard analysis. This needs more study; however, it opens the question of using the resonance frequency as a site classification proxy as it has already been done in few ground motion models in Japan and Europe.

KNET and KiK-net data are invaluable to study nonlinear processes in the top crust due to its longevity (around 20 years), site characterization, the presence of different tectonic regimes, and large recorded ground motion levels. These studies will help to better assess *in-situ* soil nonlinear behavior, which is much required in any seismic hazard analysis. We need to improve our understading of the mechanism of the nonlinear processes to have better numerical models for ground motion prediction. In a more general sense, these studies will help to comprehend the rheology of the shallow crust and the recovery after strong shaking.

ACKNOWLEDGMENTS

This study has not been possible without the work of staff and researchers at NIED. They install, maintain, and make the data available of the KNET and KiK-net networks. Many thanks to them. This study is partially funded by the Ministry of Ecology (Direction of Disaster Prevention, DPRG) of France on earthquake risk and hazard studies, and by EU Horizon 2020, project URBASIS (Project No. 813137).

REFERENCES

Bonilla, L. F., K. Tsuda, N. Pulido, J. Régnier, and A. Laurendeau (2011). Nonlinear site response evidence of K-NET and KiK-net records from the 2011 off the Pacific coast of Tohoku earthquake, *Earth Planets Space*, 63, 785-789.

Bonilla, L. F., P. Guéguen and Y. Ben-Zion (2019). Monitoring coseismic temporal changes of shallow material during strong ground motion with interferometry and autocorrelation, *Bull. Seism. Soc. Am.*, Vol. 109, No. 1, pp. 187-198, doi: 10.1785/0120180092

Bonilla, L.F. and Y. Ben-Zion (2020). Detailed space-time variations of the seismic response of the shallow crust to small earthquakes from analysis of dense array data, *Geophysical Journal International*, Vol. 225, Issue 1, pp. 298-310, https://doi.org/10.1093/gji/ggaa544

Brenguier, F., Shapiro, N.M., Campillo, M., Ferrazzini, V., Duputel, Z., Coutant, O. and Nercessian, A., (2008). Towards forecasting volcanic eruptions using seismic noise, *Nat. Geosci.* 1, 126-130, doi:10.1038/ngeo104

Brenguier, F., Campillo, M., Takeda, T., Aoki, Y., Shapiro, N.M., Briand, X., Emoto, K. and Miyake, H. (2014). Mapping pressurized volcanic fluids from induced crustal seismic velocity drops, *Science*, 345, 80-82

Claerbout, J. F. (1968). Synthesis of a layered medium from its acoustic transmission response, *Geophysics* 33, no. 2, 264–269

Di Alessandro,C., L. F. Bonilla, D. M. Boore, A. Rovelli, and O. Scotti (2012). Predominant-Period Site Classification for Response Spectra Prediction Equations in Italy, *Bull. Seismol. Soc. Am.*, Vol. 102, No. 2, pp. 680-695

Ishihara K., Soil Behaviour in Earthquake Geotechnics, Oxford University Press, p. 360, ISBN-10: 0198562241

Johnson, P. A., and Jia, X., (2005). Nonlinear dynamics, granular media and dynamic earthquake triggering, *Nature*, **473**, 871-874

Lieou, C. K. C., E. G. Daub, R. A. Guyer, and P. A. Johnson (2017), Nonlinear softening of unconsolidated granular earth materials, *J. Geophys. Res. Solid Earth*, 122, 6998–7008, doi:10.1002/2017JB014498

Nakata, N. and R. Snieder (2012). Estimating near-surface shear wave velocities in Japan by applying seismic interferometry to KiK-net data, *Journal of Geophysical Research*, 117, doi: 10.1029/2011JB008595

Okada, Y., Kasahara, K., Hori, S., Obara K., Sekiguchi S., Fujiwara H., and Yamamoto A. (2004). Recent progress of seismic observation networks in Japan —Hi-net, F-net, K-NET and KiK-net—. Earth Planet Sp 56, xv–xxviii (2004). https://doi.org/10.1186/BF03353076

Pasqualini, D., K. Heitmann, J. A. T enCate, S. Habib, D. Higdon, and P . Johnson (2007). Nonequilibrium and nonlinear dynamics in Berea and Fontainebleau sandstones: Low-strain regime, *J. Geophys. Res.* 112, no. B01204, doi: 10.1029/2006JB004264

Poupinet G., W.L. Ellworth, and J. Frechet (1984). Monitoring velocity variations in the crust using earthquake doublets: An application to the Calaveras Fault, California, *J. Geophys. Res.*, 89, 5719-5731.

Qin, L., Y. Ben-Zion, L. F. Bonilla, and J. H. Steidl (2020). Imaging and monitoring temporal changes of shallow seismic velocities at the Garner Valley near Anza, California, following the M7.2 2010 El Mayor-Cucapah earthquake, *Journal of Geophysical Research: Solid Earth*, doi: 10.1029/2019JB018070

Régnier, J., H. Cadet, L. F. Bonilla, E. Bertand, and J.F. Semblat (2013). Assessing nonlinear behavior of soil in seismic site response: Statistical analysis on KiK-net strong motion data, *Bull. Seismol. Soc. Am.* 103, no. 3, 1750-1770

Roux, P. and Y. Ben-Zion (2014). Monitoring fault zone environments with correlations of earthquake waveforms, *Geophys. J. Int.*, 196, 1073-1081, doi: 10.1093/gji/ggt441

Sattari, H. (2017). High-resolution seismic complex trace analysis byadaptive fast sparse S-transform, *Geophysics*, Vol. 82, doi: 10.1190/GEO2015-0425.1

Schimmel, M. (1999). Phase cross-correlations: Design, comparisons, and applications. *Bulletin of the Seismological Society of America*, *89*(5), 1366-1378

Sens-Schönfelder, C. and Wegler, U., (2006). Passive image interferometry and seasonal variations of seismic velocities at Merapi volcano, Indonesia, *Geophys. Res. Lett.* **33**, L21302

TenCate, J.A. (2011). Slow dynamics of earth materials: An experimental overview, *Pure and Applied Geophysics*, Vol. 168, pp. 2211-2219

Ventosa, S., M. Schimmel, and E. Stutzmann (2019). Towards the Processing of Large Data Volumes with Phase Cross-Correlation, *Seism. Res. Letters*, 90, 1663-1669

Wang, Q.Y., M. Campillo, F. Brenguier, A. Lecointre, T. Takeda and A. Hashima (2019). Evidence of Changes of Seismic Properties in the Entire Crust Beneath Japan After the Mw 9.0, 2011 Tohoku-oki Earthquake, *Journal of Geophysical Research: Solid Earth*, doi: 10.1029/2019JB017803

Wapenaar, K. (2003). Synthesis of an inhomogeneous medium from its acoustic transmission response, *Geophysics*, Vol. 68, No. 5, 1756-1759

Wapenaar, K., D. Draganov, R. Snieder, X. Campman, and A. Verdel (2010). Tutorial on seismic interferometry: Part 1 - Basic principles and applications, *Geophysics*, Vol. 75, doi: 10.1190/1.3457445

Wu, C. and Z. Peng (2012). Long-Term Change of Site response after the Mw9.0 Tohoku Earthquake in Japan, *Earth Planets Space*, 64, 1259-1266

Zhao, J. X., J. S. Hu, F. Jiang, J. Zhou, Y. Zhang, X. An, M. Lu, and D. A. Rhoades (2015). Nonlinear site models derived from 1-D analyses for ground-motion prediction equations using site class as the site parameter, *Bull. Seism. Soc. Am.*, 105, no. 4, 2010-2022.